Influence of multi-channel combination, parallel imaging, and other reconstruction techniques on MRI noise characteristics

Olaf Dietrich[1], PhD; José G. Raya[1], MSc; Scott B. Reeder[2,3], MD, PhD; Michael Ingrisch[1], MSc; Maximilian F. Reiser[2], MD; Stefan O. Schoenberg[2,4], MD

[1] Josef Lissner Laboratory for Biomedical Imaging, Department of Clinical Radiology – Grosshadern, Ludwig Maximilian University of Munich, Germany

[2] Department of Clinical Radiology – Grosshadern, Ludwig Maximilian University of Munich, Germany

[3] Department of Radiology, University of Wisconsin – Madison, WI, USA

[4] Institute of Clinical Radiology and Nuclear Medicine, University Hospital Mannheim, Medical Faculty Mannheim – University of Heidelberg, Mannheim, Germany

Final version: *Magn Reson Imaging* 2008; **26**(6): 754–762. <URL:http://dx.doi.org/10.1016/j.mri.2008.02.001>

Abstract

The statistical properties of background noise such as its standard deviation and mean value are frequently used to estimate the original noise level of the acquired data. This requires the knowledge of the statistical intensity distribution of the background signal, i.e. the probability density of the occurrence of a certain signal intensity. The influence of many new MRI techniques and in particular of various parallel-imaging methods on the noise statistics have neither been rigorously investigated nor experimentally demonstrated yet.

In this study, the statistical distribution of background noise was analyzed for MR acquisitions with a single-channel and a 32-channel coil, with sum-of-squares and spatial-matched-filter data combination, with and without parallel imaging using k-space and image-domain algorithms, with real-part and conventional magnitude reconstruction, and with several reconstruction filters. Depending on the imaging technique, the background noise could be described by a Rayleigh distribution, a non-central chi-distribution, or the positive half of a Gaussian distribution. In particular, the noise characteristics of sum-of-squares-reconstructed multi-channel acquisitions (with k-space-based parallel imaging or without parallel imaging) differ substantially from those with image-domain parallel imaging or spatial-matched-filter combination.

These effects must be taken into account if mean values or standard deviations of background noise are employed for data analysis such as determination of local noise levels. Assuming a Rayleigh distribution as in conventional MR images or a non-central chi-distribution for all multi-channel acquisitions is invalid in general and may lead to erroneous estimates of the signal-to-noise ratio or the contrast-to-noise ratio.

Keywords

Magnetic resonance imaging; Background noise; Statistical noise distribution; Parallel imaging; Multi-channel acquisition; Reconstruction filters

Corresponding author:

Olaf Dietrich, PhD
Ludwig Maximilian University of Munich
Josef Lissner Laboratory of Biomedical Imaging
Department of Clinical Radiology – Grosshadern
Marchioninistr. 15, 81377 Munich, GERMANY
Telephone number: +49 (0)89 7095-3623
Fax number: +49 (0)89 7095-4627
E-mail: od@dtrx.net

Introduction

The properties of background noise of MR images, such as the statistical intensity distribution and its mean value and standard deviation, have been discussed in several publications [1–9]. In particular, it is well known that conventional MR image acquisition with a single-channel RF coil and reconstruction by Fourier transform with subsequent magnitude calculation results in spatially homogeneously distributed image noise with Rayleigh statistics in background areas (i.e. in air) [1–9]. The statistical properties of this background noise were frequently used to estimate the noise level in foreground areas of the image, e.g. to determine the signal-to-noise ratio (SNR) [2,10] or the contrast-to-noise ratio (CNR).

However, the application of multi-channel surface coil arrays, new acquisition techniques such as parallel imaging, and certain reconstruction filters can influence the statistical distribution of image noise. In this case, the use of the signal mean value or the standard deviation of a background region will lead to inaccurate estimations of the true local noise level if a Rayleigh distribution is erroneously assumed, and SNRs determined from these parameters will be over- or underestimated [11]. The influence of many new MRI techniques and in particular of various parallel-imaging methods on the noise statistics have neither been rigorously investigated nor experimentally demonstrated yet.

The purpose of this study was to analyze the statistical noise distribution in background areas of MR magnitude images for several imaging techniques today commonly encountered in clinical practice such as data acquisition with multi-channel coil arrays, parallel imaging, and various reconstruction filters.

Theory

In MRI, the real and imaginary part of the acquired complex raw data in k-space are usually assumed to be superimposed by Gaussian (i.e. normally) distributed noise. The complex image data of a single receiver channel reconstructed by Fourier transform will then also be superimposed by normally distributed noise [3,4]. After calculating the magnitude of this complex image, the signal is described by a Rician distribution [2,3,7,9] in general and a Rayleigh distribution [1] in the image background. If data are acquired by multi-channel phased-array coils [12] and reconstructed as root of the sum of squares of the complex images of each channel, then noise properties are described by the non-central χ-distribution [8,9]. Mathematical details of these statistical distributions are presented in the Appendix.

An alternative to the sum-of-squares (SoS) reconstruction of multi-channel data from phased-array coils is the "spatial matched filter" (SMF) approach, which is the optimal coil combination method with a maximized SNR of the resulting image [12,13]. The SMF approach linearly combines complex image data from different receiver channels weighted by coefficients derived from the locally varying coil sensitivities and the noise correlation matrix. Thus, a single intermediary complex image is reconstructed as (pixel-wise) linear combination of the multi-channel data before the final calculation of the magnitude image. As a consequence of the Gaussian noise distribution in the intermediary complex image, a Rayleigh distribution is expected in the final magnitude image.

A very important technique for accelerated MRI is parallel imaging using either frequency-domain methods such as the generalized auto-calibrating partially parallel acquisition (GRAPPA) algorithm [14] or image-domain methods such as sensitivity-encoded MRI (SENSE) [15]. All parallel-imaging techniques are based on an undersampled acquisition of raw data and incorporation of the coil-sensitivity profiles into the image-reconstruction process. The GRAPPA algorithm first calculates the missing k-space lines before full-FOV images for each receiver channel are reconstructed. These images can be combined exactly as conventional multi-channel data using either the sum-of-squares or spatial-matched-filter technique, resulting in noise distributions as described above. The SENSE algorithm reconstructs complex images with aliasing artifacts for each receiver channel; these images are then (pixel-wise) linearly combined to one complex full-FOV image. Thus, the final magnitude image has noise properties as in the case of an SMF reconstruction, i.e. a Rayleigh distribution is expected.

In certain situations, data are reconstructed as real-part images instead of complex-magnitude images. In most cases, the real-part reconstruction is preceded by a phase correction to avoid image artifacts due to imaginary signal contributions. Real-part images are desirable, for instance, in inversion-recovery experiments in order to preserve the sign of the longitudinal magnetization. Another common technique that can result in real-part reconstructed images is half-Fourier MRI with the Margosian algorithm [16]. The Margosian algorithm includes an intrinsic phase-correction, which invalidates the information of the imaginary channel, and is therefore typically followed by a real-part reconstruction. In this case, a real-part image with normally distributed noise is reconstructed and negative data are removed by magnitude calculation afterwards. This reconstruction results in background noise described by the positive part of a Gaussian distribution with mean value 0. Multi-channel real-part data can also be combined with either the spatial-matched-filter method, which results in the same noise characteristics as in a corresponding single-channel acquisition, or with the sum-of-squares method, which is equivalent to a sum-of-squares reconstruction of complex image data with half the number of channels. This can be seen by comparing the sum of squares $\sum_{c=1}^{n} \Re(a_c(\mathbf{r}))^2$ of an *n*-channel real-part image at position $\mathbf{r}$ ($\Re(a_c(\mathbf{r}))$ denotes the real part of the image intensity of channel $c = 1 \ldots n$) and the sum of squares of conventional multi-channel data $\sum_{c=1}^{n} |a_c(\mathbf{r})|^2 = \sum_{c=1}^{n} \left(\Re(a_c(\mathbf{r}))^2 + \Im(a_c(\mathbf{r}))^2 \right) = \sum_{c=1}^{n} \Re(a_c(\mathbf{r}))^2 + \sum_{c=1}^{n} \Im(a_c(\mathbf{r}))^2$, since the noise properties of the real parts, $\Re(\cdot)$, and the imaginary parts, $\Im(\cdot)$, are the same.

Reconstruction filters can also influence the statistical noise distribution. Filters considered in this study as typical examples that demonstrate this behavior are raw-data filters such as a Hanning filter, an intensity-normalization filter, and a large-field-of-view (large-FOV) correction filter, which is also known as gradient-warp correction. Raw-data filters work by multiplication of the k-space data with a weighting function. The Hanning filter, for instance, provides higher weighting to central k-space data and lower weighting to peripheral k-space data. This filter increases the SNR and reduces edge ringing, however, the spatial image resolution is also decreased to a certain degree. The effect of this filter on the signal statistics can be understood by considering that a multiplication in the frequency domain is equivalent to a convolution of the complex image data with the Fourier-transformed filter. Thus, the complex image data after raw-data filtering is a weighted sum (convolution) of the original data points. If the convolution kernel is sufficiently small, which is the case for typical raw-data filters, then only neighboring pixels are convolved. Hence, a pixel in the background is calculated as weighted sum of the background pixels in its neighborhood and therefore the superimposed noise remains normally distributed, but, generally, with a reduced standard deviation.

The intensity-normalization filter is used to compensate for a spatially varying intensity distribution caused by inhomogeneous coil profiles, which are typical for surface-coil systems. This filter works in the image domain and multiplies the image data with a slowly varying correction function. If the region of interest used for statistical analysis is sufficiently small (relative to the spatial variation of the filter), then the noise distribution remains Gaussian and only its standard deviation will be changed. Thus, for both the raw-data and the intensity-normalization filters, background noise of magnitude images is expected to follow (at least approximately) a Rayleigh distribution.

The large-FOV compensation filter is used to correct geometric distortions such as “pin-cushion” distortions at the edges of the FOV due to gradient non-linearity. The spatial-distortion algorithm works on the final magnitude images and interpolates new pixels as well as discards existing pixels, followed by an intensity correction based on the Jacobian of the distortion [17,18]. The effect of the large-FOV compensation is maximal at the edges of the field of view, i.e. in areas that typically belong to the image background. Since the extent and direction of the distortion correction can vary substantially within relatively small distances close to the edges of the FOV, even small background regions will be affected by complex non-linear signal-distortion effects. Thus, the large-FOV compensation must be expected to influence not only the standard deviation of noise but also the shape of the statistical distribution. All noise distributions considered in this section are summarized in Table 1.

Table 1: Statistical background-noise distributions in magnitude images[a]

Acquisition/reconstruction technique	Complex magnitude data	Real-part data
Single-channel acquisition	Rayleigh distrib.	Half-Gaussian distrib.
Multi-channel (*n*), sum-of-squares reconstruction	Non-central χ-distrib. (*n*)	Non-central χ-distrib. (*n*/2)
Multi-channel (*n*), spatial-matched filter reconstruction	Rayleigh distrib.	Half-Gaussian distrib.
Multi-channel (*n*), sum-of-squares GRAPPA	Non-central χ-distrib. (*n*)	Non-central χ-distrib. (*n*/2)
Multi-channel (*n*), spatial-matched filter GRAPPA	Rayleigh distrib.	Half-Gaussian distrib.
Multi-channel (*n*), SENSE	Rayleigh distrib.	Half-Gaussian distrib.
Raw-data filter	Unchanged distrib.	Unchanged distrib.
Intensity-normalization filter	Unchanged distrib.	Unchanged distrib.
Large-FOV filter	Modified distrib.	Modified distrib.

[a] *n* denotes the number of channels in multi-channel acquisitions.

Materials and Methods

Phantom experiments were performed on a 3-T whole-body MRI system (Magnetom Tim Trio, Siemens Medical Solutions, Erlangen, Germany) using a single-channel volume body coil (1CH) and a dedicated cardiovascular 32-channel surface-coil array (32CH) (Rapid Biomedical, Rimpar, Germany) consisting of 32 independent coil elements (16 posterior and 16 anterior) matching the 32 receiver channels of the MRI system. The cylindrical liquid phantom had a diameter of 20 cm and a length of 30 cm.

Using the single-channel body coil, only acquisitions without parallel imaging were performed. Image reconstruction was performed without filtering as well as with a Hanning filter, a large-FOV correction filter, and an intensity-normalization filter.

Using the 32-channel coil, phantom images were acquired with the GRAPPA algorithm [14], with a modified sensitivity-encoding (mSENSE) algorithm [19], and without parallel imaging. The parallel-imaging acceleration factor was $R = 4$ and the number of reference lines for auto-calibration and the calculation of the coil sensitivity profiles was 32. 32-channel data of non-accelerated and GRAPPA acquisitions were reconstructed with the sum-of-squares and the spatial-matched-filter approach, which is provided as "adaptive combine" on the employed MRI scanner.

Two different pulse sequences were used in this study: a fully gradient-balanced steady-state free-precession (SSFP) sequence and a spin-echo-based single-shot half-Fourier-acquired "rapid acquisition with relaxation enhancement" (hF-RARE) sequence, which is provided under the acronym HASTE (for "half-Fourier-acquisition single-shot turbo-spin-echo) on the employed MRI scanner. The hF-RARE sequence with Margosian reconstruction was chosen as example for a phase-corrected real-part reconstruction with subsequent magnitude calculation. For both sequences, we acquired one slice in transverse orientation with a square FOV of 300×300 mm^2, a slice thickness of 5 mm, and phase-encoding direction from left to right. The matrix size was 256×256 for all acquisitions. For the SSFP sequence, we used a TR of 3.9 ms, TE of 1.95 ms, and a bandwidth of 930 Hz/pixel acquiring the full k-space in phase-encoding direction. For the hF-RARE sequence, we used a TR of 1000 ms, TE of 94 ms, and a bandwidth of 490 Hz/pixel, acquiring 4/8 (50 %) of the k-space in phase-encoding direction plus 16 additional lines required for phase correction of the Margosian reconstruction and for coil calibration when parallel imaging was applied.

A rectangular region (area 128×32 = 4096 pixels) was positioned outside the phantom (close to the image edge in readout direction) to analyze the background noise of the magnitude images. Intensity histograms were used to evaluate the noise characteristics. We compared the histogram data with the Rayleigh distribution [1], with a half-Gaussian distribution, and with the non-central χ-distribution [8]. The original standard deviation, σ, of these distributions was derived from the mean values and standard deviations of the actual intensity data using Eqs. (9) and (16b) of the Appendix; in the case of the half-Gaussian distributions, we synthesized the negative half of the distribution before calculating the standard deviation. The parameter *n* describing the effective number of receiver channels in the sum-of-squares reconstruction was determined by

comparing the ratio of the mean value and standard deviation of the background signal with Table 2.

Table 2: Background noise characteristics based on non-central χ-distribution

Number of coil elements	Noise mean value (σ = 1)	Noise standard deviation (σ = 1)	Ratio (mean value/ std. dev.)
1	1.253	0.6551	1.913
2	1.880	0.6824	2.755
3	2.350	0.6911	3.400
4	2.742	0.6953	3.943
5	3.084	0.6978	4.420
6	3.393	0.6994	4.851
7	3.675	0.7005	5.246
8	3.938	0.7014	5.615
9	4.184	0.7020	5.960
10	4.417	0.7026	6.287
11	4.637	0.7030	6.596
12	4.848	0.7033	6.893
13	5.050	0.7036	7.177
14	5.244	0.7039	7.450
15	5.432	0.7041	7.715
16	5.613	0.7043	7.970
18	5.958	0.7046	8.456
20	6.285	0.7049	8.917
22	6.596	0.7051	9.355
24	6.892	0.7052	9.773
26	7.177	0.7054	10.175
28	7.450	0.7055	10.560
30	7.714	0.7056	10.932
32	7.969	0.7057	11.292
36	8.456	0.7059	11.980
40	8.916	0.7060	12.629
44	9.354	0.7061	13.248
48	9.772	0.7062	13.838
52	10.174	0.7063	14.406
56	10.559	0.7063	14.949
60	10.932	0.7064	15.476
64	11.292	0.7064	15.985

The quantitative comparison of noise data and statistical noise distributions was performed with a χ^2-technique: Noise data were sorted into 16 *non-equally spaced* bins that were defined such that the pixel number $N_i, i = 1 \ldots 16$, in each bin was about $256 = 4096/16$. (Consequently, bins were narrow for signal intensities that were observed frequently and wide at the tails of the intensity distribution.) We calculated χ^2 as

$$\chi^2 = \sum_{i=1}^{16} \frac{(N_i - e_i)^2}{N_i} \quad (1)$$

where e_i denotes the theoretically expected number of pixels in bin i according to the intensity distribution used for comparison. If the theoretical model agrees with the measured data, the probability for a $\chi^2 \geq 26.3$ is lower than 0.05 (for 16 bins, i.e. 16 degrees of freedom); thus, $\chi^2 < 26.3$ represents an agreement of the theoretical model and the observed noise distribution.

Results

Histograms of background noise for all used pulse sequences are shown in Figs. 1 and 2. Background noise of the unfiltered SSFP measurement with the single-channel coil agrees very well with the Rayleigh statistics (Fig. 1a). Applying the Hanning or the intensity-normalization filter influences the standard deviation but not the general form of the noise distribution, while the application of the large-FOV filter results in a slightly modified noise distribution, which is indicated, for instance, by the non-identical Rayleigh curves derived from the mean value (solid) and the standard deviation (dashed) of the noise data (Figs. 1d–f).

The noise distributions of the SSFP measurements with the 32-channel coil depend on the applied reconstruction technique: after sum-of-squares reconstruction (without acceleration or with GRAPPA), an approximate non-central χ-distribution was found (Figs. 1b,g), while the spatial-matched-filter and mSENSE reconstruction resulted in background noise with an approximate Rayleigh distribution (Figs. 1c,h,i).

Background noise of the hF-RARE acquisitions with the single-channel coil as well as with mSENSE or spatial-matched-filter reconstruction could be approximated by half-Gaussian distributions (Figs. 2a,c,d,f,h,i) with mean value of 0; obvious deviations were found only after application of the large-FOV filter (Fig. 2e). hF-RARE measurements with sum-of-squares reconstruction were visually well described by a non-central χ-distribution (Figs. 2b,g).

In the case of non-central χ-distributions, the effective numbers of channels determined from the ratio of mean value and standard deviation of the noise data

were 12 and 6 for the SSFP sequence with sum-of-squares reconstruction and acceleration factors of 1 and 4, respectively. The corresponding effective numbers of channels were 7 and 3 for the hF-RARE measurements.

The χ^2-values describing the deviation between observed background noise distributions and theoretical distributions are listed in Table 3. For the SSFP measurements with the single-channel coil, the Rayleigh distribution (and equivalently the non-central χ-distribution for 1 channel) agrees well ($\chi^2 < 26.3$) with the noise data acquired without filter, with Hanning filter, or with intensity-normalization filter. For the hF-RARE sequence, the corresponding acquisitions agree equally well with the positive half of a Gaussian distribution. In all acquisitions with sum-of-squares reconstruction, moderate values of χ^2 (< 400) were observed, which were substantially lower than the χ^2 for Rayleigh distributions with the same standard deviation or mean value.

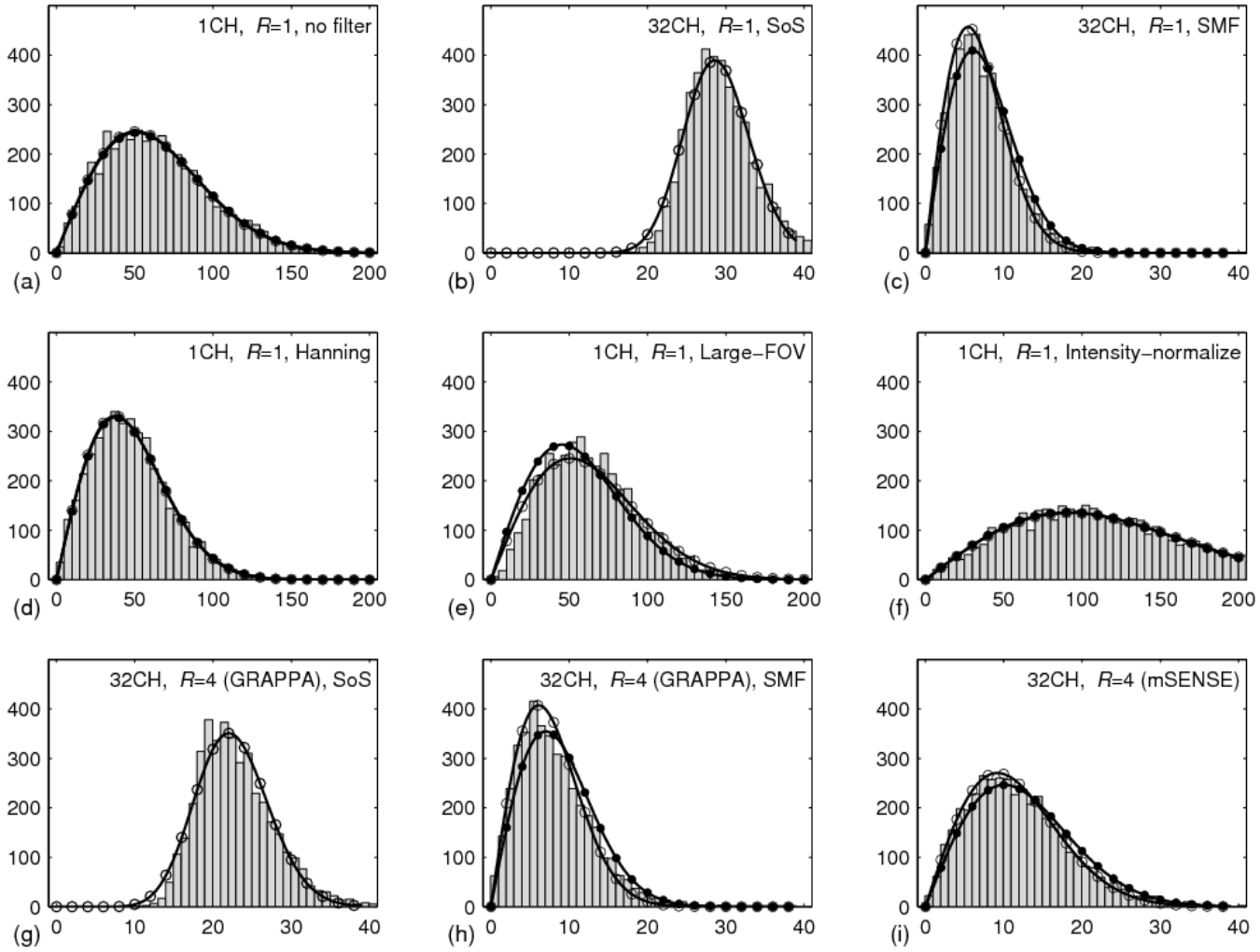

Figure 1: Histograms of intensity distributions of background noise in measurements with an SSFP sequence. The black lines with open and filled circles in plots (a), (c), (d), (e), (f), (h), and (i) show Rayleigh distributions based on the standard deviation and the mean value of the noise distribution, respectively. The black lines with open circles in plots (b) and (g) show non-central χ-distributions calculated from the standard deviation and the mean value of the histogram data. Data were acquired with a 1-channel (1CH) and 32-channel (32CH) coil, using parallel-imaging acceleration factors of R = 1 and 4, different reconstruction techniques (sum of squares (SoS), spatial matched filter (SMF), GRAPPA, mSENSE), and different reconstruction filters (Hanning filter, large-FOV filter, intensity-normalization filter).

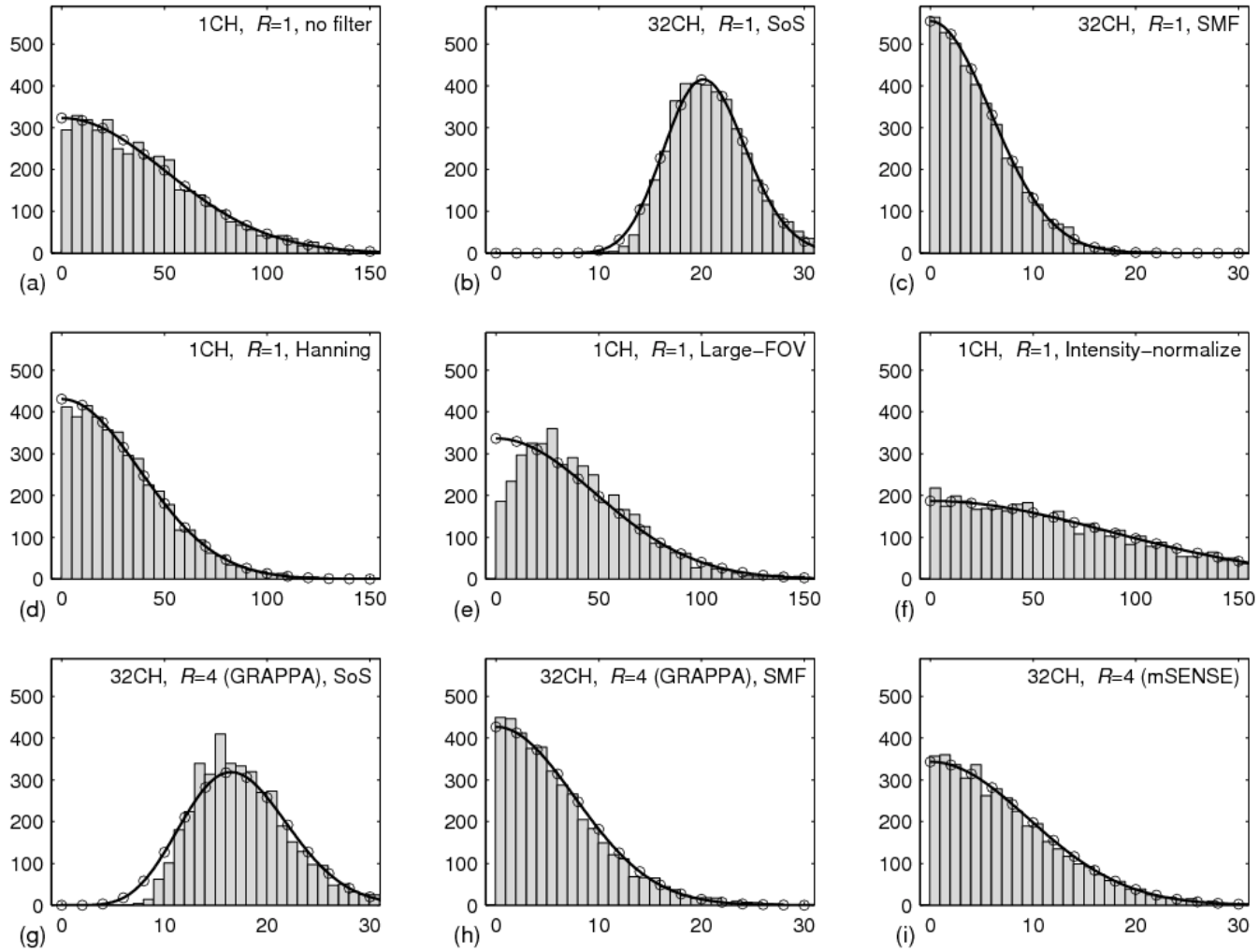

Figure 2: Histograms of intensity distributions of background noise in measurements with an hF-RARE sequence with real-part reconstruction. The black lines in plots (a), (c), (d), (e), (f), (h), and (i) show half-Gaussian distributions calculated from the standard deviation of the histogram data. The black line in plots (b) and (g) show non-central χ-distributions calculated from the mean value and standard deviation of the histogram data. Data were acquired with a 1-channel (1CH) and 32-channel (32CH) coil, using different parallel-imaging acceleration factors of R = 1 and 4, and different reconstruction techniques as listed in the caption of Fig. 1.

Discussion

Our histogram analysis demonstrates that the background noise follows with reasonable accuracy the expected statistical distributions as summarized in Table 1: Single-channel, spatial-matched-filter, and mSENSE reconstructions result in approximately normally distributed noise prior to the final magnitude calculation. If real and imaginary parts are used in the final step (as in the SSFP measurements), background noise follows a Rayleigh distribution; if only the real part is used (as in the hF-RARE measurements) it follows a half-Gaussian distribution.

Table 3: χ^2-values describing the difference between observed noise distributions and theoretical models[a]

Pulse sequence	Acquisition/reconstruction technique	Rayleigh (std.dev.)	Rayleigh (mean val.)	non-central χ-distribution	half-Gaussian distribution
SSFP	1CH, *R*=1, no filter	**15**	**13**	**14**	*10565*
	32CH, *R*=1, SoS	*17537*	*91969*	172	*92325*
	32CH, *R*=1, AdC	79	47	44	*10033*
	1CH, *R*=1, Hanning	**18**	**16**	**17**	*10671*
	1CH, *R*=1, Large-FOV	147	357	155	*19445*
	1CH, *R*=1, Intensity-normalize	**21**	**22**	**21**	*11887*
	32CH, *R*=4 (GRAPPA), SoS	*9707*	*72353*	168	*88435*
	32CH, *R*=4 (GRAPPA), AdC	95	114	57	*8860*
	32CH, *R*=4 (mSENSE)	36	54	**20**	*9504*
hF-RARE	1CH, *R*=1, no filter	*898*	*1547*	*825*	**25**
	32CH, *R*=1, SoS	*12145*	*77620*	122	*87044*
	32CH, *R*=1, AdC	*1115*	*1776*	921	**18**
	1CH, *R*=1, Hanning	*843*	*1464*	*758*	**17**
	1CH, *R*=1, Large-FOV	*408*	*823*	*379*	216
	1CH, *R*=1, Intensity-normalize	*980*	*1697*	*910*	**15**
	32CH, *R*=4 (GRAPPA), SoS	*5945*	*35755*	368	*83179*
	32CH, *R*=4 (GRAPPA), AdC	*1116*	*2128*	*1018*	32
	32CH, *R*=4 (mSENSE)	*1086*	*1931*	*956*	**17**

[a] bold numbers denote values of $\chi^2<26.3$, corresponding to a $p>.05$ for 16 degrees of freedom; italic numbers denote comparisons for which no agreement was expected.

32-channel acquisitions reconstructed with a sum-of-squares algorithm result in background noise described by a non-central χ-distribution. This is true for both, conventional 32-channel acquisitions as well as parallel-imaging acquisitions with the GRAPPA algorithm and subsequent sum-of-squares reconstruction. As expected, the effective numbers of channels derived from the ratio of mean value and standard deviation of the noise data demonstrate a reduction by a factor of about 2 in the case of the real-part-only sum-of-squares reconstruction (hF-RARE measurements) compared to the sum-of-squares reconstruction with real and imaginary part (SSFP measurements). In both cases, however, the effective numbers of channels (ranging between 3 and 12) are considerably lower than 32, which is the actual number of channels used for the acquisition. We assume that this effect is caused by noise correlation between receiver channels (i.e. non-independent noise), which influences the noise standard deviation of sum-of-squares images as described by Constantinides et al. [8].

The χ^2-values for the non-central χ-distributions of sum-of-squares-reconstructed data vary between 122 and 368 indicating some remaining (relatively small) systematic deviations between the observed noise distributions and the statistical model. These deviations can also be explained by correlated noise received with the 32-channel array. A perfect non-central χ-distribution can only be expected for independent noise in all channels [8], and our introduction of a reduced effective number of coil elements is an empirical ad-hoc solution, which cannot be expected to result in perfect agreement of measurement and theory. Similar deviations are observed for several 32-channel acquisitions with the spatial-matched-filter or mSENSE reconstruction. Although noise correlation should be compensated in these reconstructions, the accuracy of the correlation matrices determined from noise prescans may not be sufficient for a complete noise decorrelation.

A potential further source of statistical deviations is the size of the evaluated background region. If the background noise is distributed non-uniformly, the noise level may vary substantially within the assessed background region and areas with different noise levels are averaged. Consequently, the noise properties may not longer be described by a simple statistical distribution. The relatively small differences between

the histogram data and the model distributions in Figs. 1 and 2, however, demonstrate that the noise variations within the assessed regions are relatively small, although they may explain some of the observed deviations of the χ^2-values in Table 3.

The mSENSE implementation used in this study can be expected to exhibit the same general signal statistics as the original SENSE implementation; the crucial property common to both approaches is that complex image data of several channels are pixel-wise linearly combined before the final magnitude calculation, which results in Rician signal statistics. However, certain differences may occur between both implementations with respect to the background noise because of the different techniques used for the determination of the coil sensitivity profiles. If the coil sensitivity maps are restricted to the imaged foreground object plus a small extrapolation zone as suggested in the original SENSE implementation [15], no meaningful signal can be calculated in the image background. In this case the final image is frequently masked to the foreground object plus the extrapolation zone, and the remaining background signal is set to zero. If, on the other hand, the coil sensitivity profiles are extrapolated (e.g., using polynomial fitting) to the full field of view as in mSENSE, then background noise will be Rayleigh-distributed as demonstrated in this study.

If the statistical noise distribution is known, the original standard deviation σ can locally be determined from the standard deviation and/or mean value of the background noise as outlined in the Appendix. This is demonstrated by the excellent agreement of the curves with filled and open symbols e.g. in Figs. 1a,d,f. It should be noted, however, that σ can only be used for SNR or CNR determinations if the background noise is spatially uniform, i.e. if the background noise is representative for the whole image. This is generally not true for parallel-imaging acquisitions or after application of filters such as the intensity-normalization filter [11]. In parallel imaging, the noise amplification and the resulting non-uniform noise distribution is described by the geometry factor (g-factor) [15], which depends, e.g., on the image and coil geometry, the reduction factor, and the applied parallel-imaging algorithm as recently demonstrated for SENSE and GRAPPA [20]. The effect of certain reconstruction filters on the background noise can also be described by a spatially varying scaling factor. Only if these scaling factors (g-factor or filter scaling) can be obtained as parameter maps from the image-reconstruction system, it becomes possible again to employ the local standard deviation of the background noise for SNR or CNR measurements. This can be done by correcting the locally measured original standard deviation σ of the evaluated background region with the ratio of the scaling factors in the foreground region of interest and the assessed background region.

In conclusion, the statistical signal distribution of background noise depends on applied reconstruction filters, the number of receiver channels, and the chosen conventional or parallel-imaging reconstruction technique. These effects must be taken into account if mean values or standard deviations of background noise are employed for data analysis such as determination of local noise levels. Assuming a Rayleigh distribution as in conventional MR images or a non-central χ-distribution for all multi-channel acquisitions is invalid in general and may lead to erroneous estimates of SNR or CNR.

Appendix: Statistical signal distributions in the presence of noise

In the presence of noise, the signal distribution in an MR image is described by a statistical distribution whose exact form depends on the data acquisition and image reconstruction methods. We assume that the noise superimposing the real and imaginary part of the complex raw data (of each receiver channel) in k-space has a Gaussian distribution with mean value of zero. If the complex data (of a single receiver channel) are reconstructed by a Fourier transform, the real and imaginary part of the resulting complex image data are also superimposed by normally distributed noise [3,4] described by the probability distribution P for the signal x:

$$P(x;\mu,\sigma) = \frac{1}{\sqrt{2\pi}\,\sigma}\exp\frac{-(x-\mu)^2}{2\sigma^2} \qquad (2)$$

with standard deviation σ and mean value μ (the mean values of the real part and the imaginary part will in general be different; in background areas, this mean value, μ, is zero). The standard deviation σ of this Gaussian distribution will be referred to as "original

standard deviation σ", since the actual standard deviation measured in the background of a magnitude image, will be different from σ, in general.

Magnitude images, one receiver channel

Typical MR images are magnitude images calculated from intermediary complex image data. After magnitude calculation, the signal distribution in a region with original signal S (i.e., the signal without noise) is described by the Rician distribution [2,3,7,9,21]:

$$P_{\mathrm{Ri}}(x;S,\sigma)=\frac{1}{\sigma^2}\,x\exp\left(\frac{-\left(x^2+S^2\right)}{2\sigma^2}\right)I_0\left(\frac{xS}{\sigma^2}\right) \quad (3)$$

where $I_n(z)$ is the modified Bessel function of the first kind of nth order. Mean value, m_{Ri}, and standard deviation, s_{Ri}, of this distribution are:

$$m_{\mathrm{Ri}}=\sqrt{\frac{\pi}{2}}\,\sigma\exp\left(\frac{-S^2}{4\sigma^2}\right)\times\left(\left(1+\frac{S^2}{2\sigma^2}\right)I_0\left(\frac{S^2}{4\sigma^2}\right)+\frac{S^2}{2\sigma^2}I_1\left(\frac{S^2}{4\sigma^2}\right)\right) \quad (4)$$

$$s_{\mathrm{Ri}}=\sqrt{2\sigma^2+S^2-m_{\mathrm{Ri}}^2}\,. \quad (5)$$

An important special case of the Rician distribution is the signal distribution in a background area of a magnitude image, i.e., in areas with $S = 0$. In this case, the signal is described by the Rayleigh distribution [1]:

$$P_{\mathrm{Ra}}(x;\sigma)=P_{Ri}(x;0,\sigma)=\frac{1}{\sigma^2}\,x\exp\frac{-x^2}{2\sigma^2}\,. \quad (6)$$

Mean value, m_{Ra}, and standard deviation, s_{Ra}, of the Rayleigh distribution are:

$$m_{\mathrm{Ra}}=\sqrt{\frac{\pi}{2}}\,\sigma\approx 1.25\,\sigma \quad (7)$$

$$s_{\mathrm{Ra}}=\sqrt{2-\frac{\pi}{2}}\,\sigma\approx 0.655\,\sigma\,. \quad (8)$$

Consequently, the original standard deviation σ can be determined by measuring either the mean value m_{Ra} or the standard deviation s_{Ra} of the signal distribution in the image background using an appropriate correction factor:

$$\sigma=\sqrt{\frac{2}{\pi}}\,m_{\mathrm{Ra}}=\sqrt{\frac{2}{4-\pi}}\;s_{\mathrm{Ra}}\,. \quad (9)$$

Sum-of-squares reconstruction, multiple receiver channels

In the case of multiple receiver channels, the simplest and most frequently used image reconstruction is the sum-of-squares reconstruction [12,13,22]. If this reconstruction is applied to complex image data, the image signal is described by the non-central χ-distribution [8,9]:

$$P_{\mathrm{nc}\chi}(x;S,\sigma,n)=\frac{S}{\sigma^2}\left(\frac{x}{S}\right)^n\times\exp\left(\frac{-\left(x^2+S^2\right)}{2\sigma^2}\right)I_{n-1}\left(\frac{xS}{\sigma^2}\right) \quad (10)$$

where n is the number of receiver channels. The mean value of the non-central χ-distribution is

$$m_{\mathrm{nc}\chi}=\frac{1\cdot 3\cdot 5\cdots(2n-1)}{2^{n-1}(n-1)!}\sqrt{\frac{\pi}{2}}\,\sigma\times{}_1F_1\left(-\frac{1}{2},n,\frac{-S^2}{2\sigma^2}\right) \quad (11)$$

where ${}_1F_1(a, b, z)$ is the confluent hypergeometric function, and its standard deviation is

$$s_{\mathrm{nc}\chi}=\sqrt{2n\sigma^2+S^2-m_{\mathrm{nc}\chi}^2}\,. \quad (12)$$

The Rician distribution in Eq. (3) is a special case of this distribution for $n = 1$. Therefore, the non-central χ-distribution is sometimes referred to as "generalized Rician distribution".

In the image background (i.e., for $S = 0$), one can use the limiting form $I_n(z)\approx\left(\frac{z}{2}\right)^n/\Gamma(n+1)$ of the Bessel function for small $z\to 0$ [23] to simplify Eq. (10) to [8]

$$P_{\mathrm{nc}\chi}(x;0,\sigma,n)=\frac{1}{\Gamma(n)\sigma^2}\left(\frac{x}{2\sigma^2}\right)^{n-1}\times\quad x^n\exp\left(\frac{-x^2}{2\sigma^2}\right) \quad (13)$$

with the mean value (applying ${}_1F_1(a, b, 0) = 1$ [23])

$$m_{\mathrm{nc}\chi,S=0}=\frac{1\cdot 3\cdot 5\cdots(2n-1)}{2^{n-1}(n-1)!}\sqrt{\frac{\pi}{2}}\,\sigma \quad (14)$$

and standard deviation

$$s_{\mathrm{nc}\chi,S=0}=\sqrt{2n\sigma^2-m_{\mathrm{nc}\chi,S=0}^2}=\sqrt{2n-\left(\frac{1\cdot 3\cdot 5\cdots(2n-1)}{2^{n-1}(n-1)!}\right)^2\frac{\pi}{2}}\;\sigma. \quad (15)$$

Consequently, the original standard deviation σ can again be determined by measuring the mean value $m_{\mathrm{nc}\chi,S=0}$ and/or the standard deviation $s_{\mathrm{nc}\chi,S=0}$ of the signal distribution in the image background

$$\sigma=\frac{2^{n-1}(n-1)!}{1\cdot 3\cdot 5\cdots(2n-1)}\sqrt{\frac{2}{\pi}}\,m_{\mathrm{nc}\chi,S=0}\,, \quad (16a)$$

$$\sigma = \sqrt{\frac{s^2_{\mathrm{nc}\chi,S=0} + m^2_{\mathrm{nc}\chi,S=0}}{2n}}\,, \qquad (16b)$$

$$\sigma = \frac{1}{\sqrt{2n - \left(\frac{1\cdot 3\cdot 5\cdots(2n-1)}{2^{n-1}(n-1)!}\right)^2 \frac{\pi}{2}}}\, s_{\mathrm{nc}\chi,S=0}\,. \qquad (16c)$$

The factors of Eqs. (14) and (15) describing the mean values and standard deviations for different numbers of receiver channels are listed in Table 2.

The noise properties presented in Eq. (13) to (16) are valid only if the noise in the n receiver channels is completely uncorrelated. However, even if this is not the case, the second moment of the measured pixel intensities in a background region with N pixels, $E(x^2) = \left(\sum_{k=1\ldots N} x_k^2\right)/N = 2n\sigma^2$, remains unaffected by noise correlation and can be used to determine the original standard deviation as [8]

$$\sigma = \sqrt{\frac{E(x^2)}{2n}}\,. \qquad (17)$$

Acknowledgments

This study was supported in parts by the "Verein MagnetresonanzForschung e.V."

References

1. Edelstein WA, Bottomley PA, Pfeifer LM. A signal-to-noise calibration procedure for NMR imaging systems. Med Phys 1984;11:180–5.
2. Henkelman RM. Measurement of signal intensities in the presence of noise in MR images. Med Phys 1985;12:232–3.
3. Holden JE, Halama JR, Hasegawa BH. The propagation of stochastic pixel noise into magnitude and phase values in the Fourier analysis of digital images. Phys Med Biol 1986;31:383–96.
4. Bernstein MA, Thomasson DM, Perman WH. Improved detectability in low signal-to-noise ratio magnetic resonance images by means of a phase-corrected real reconstruction. Med Phys 1989;16:813–7.
5. Miller AJ, Joseph PM. The use of power images to perform quantitative analysis on low SNR MR images. Magn Reson Imaging 1993;11:1051–6.
6. McGibney G, Smith MR. An unbiased signal-to-noise ratio measure for magnetic resonance images. Med Phys 1993;20:1077–8.
7. Gudbjartsson H, Patz S. The Rician distribution of noisy MRI data. Magn Reson Med 1995;34:910–4. (Erratum in: Magn Reson Med 1996;36:332.)
8. Constantinides CD, Atalar E, McVeigh ER. Signal-to-noise measurements in magnitude images from NMR phased arrays. Magn Reson Med 1997;38:852–7. (Erratum in: Magn Reson Med 2004;52:219.)
9. Kellman P, McVeigh ER. Image reconstruction in SNR units: a general method for SNR measurement. Magn Reson Med 2005;54:1439–47.
10. Kaufman L, Kramer DM, Crooks LE, Ortendahl DA. Measuring signal-to-noise ratios in MR imaging. Radiology 1989;173:265–7.
11. Dietrich O, Raya JG. Reeder SB, Reiser MF, Schoenberg SO. Measurement of signal-to-noise ratios in MR images: Influence of multichannel coils, parallel imaging, and reconstruction filters. J Magn Reson Imaging 2007;26:375–85.
12. Roemer PB, Edelstein WA, Hayes CE, Souza SP, Mueller OM. The NMR phased array. Magn Reson Med 1990;16:192–225.
13. Walsh DO, Gmitro AF, Marcellin MW. Adaptive reconstruction of phased array MR imagery. Magn Reson Med. 2000;43:682–90.
14. Griswold MA, Jakob PM, Heidemann RM, Nittka M, Jellus V, Wang J, Kiefer B, Haase A. Generalized autocalibrating partially parallel acquisitions (GRAPPA). Magn Reson Med 2002;47:1202–10.
15. Pruessmann KP, Weiger M, Scheidegger MB, Boesiger P. SENSE: sensitivity encoding for fast MRI. Magn Reson Med 1999;42:952–62.
16. Margosian P, Schmitt F, Purdy D. Faster MR imaging: imaging with half the data. Health Care Instrum 1986;1:195–7.
17. Doran SJ, Charles-Edwards L, Reinsberg SA, Leach MO. A complete distortion correction for MR images: I. Gradient warp correction. Phys Med Biol 2005;50:1343–61.
18. Wang D, Doddrell DM, Cowin G. A novel phantom and method for comprehensive 3-dimensional measurement and correction of geometric distortion in magnetic resonance imaging. Magn Reson Imaging 2004;22:529–42.
19. Griswold MA, Kannengiesser S, Heidemann RM, Wang J, Jakob PM. Field-of-view limitations in parallel imaging. Magn Reson Med 2004;52:1118–26.
20. Thunberg P, Zetterberg P. Noise distribution in SENSE- and GRAPPA-reconstructed images: a computer simulation study. Magn Reson Imaging 2007;25:1089–94.
21. Rice SO. Mathematical analysis of random noise. In: Wax N, editor. Selected papers on noise and stochastic processes. New York: Dover Publications, 1954. p. 133–294.
22. Larsson EG, Erdogmus D, Yan R, Principe JC, Fitzsimmons JR. SNR-optimality of sum-of-squares reconstruction for phased-array magnetic resonance imaging. J Magn Reson 2003;163:121–3.
23. Abramowitz M, Stegun IA, editors. Handbook of mathematical functions with formulas, graphs, and mathematical tables. 10th printing. United States Department of Commerce. National Bureau of Standards, Applied Mathematics Series 55, 1972.